Bulletin of Volcanology
© Springer-Verlag 2003
DOI 10.1007/s00445-003-0301-2

Research Article

Erosion by flowing lava: geochemical evidence in the Cave Basalt, Mount St. Helens, Washington

David A. Williams (✉) · Steven D. Kadel · Ronald Greeley · C. Michael Lesher · Michael A. Clynne

D. A. Williams · S. D. Kadel · R. Greeley
Department of Geological Sciences, Arizona State University, Tempe, AZ 85287-1404, USA

C. M. Lesher
Mineral Exploration Research Centre, Department of Earth Sciences, Laurentian University, Sudbury, Ontario, P3E2C6, Canada

M. A. Clynne
United States Geological Survey, Menlo Park, CA 94025, USA

D. A. Williams
Present address: Department of Geological Sciences, Arizona State University, Bateman Physical Sciences F686, Box 871404 , Tempe, AZ 85287–1404, USA

✉ D. A. Williams
Phone: +1-480-9657029
Fax: +1-480-9658102
E-mail: David.Williams@asu.edu

Received: 25 July 2002 / **Accepted:** 30 May 2003 / **Published online:** 7 August 2003

Abstract We sampled basaltic lava flows and underlying dacitic tuff deposits in or near lava tubes of the Cave Basalt, Mount St. Helens, Washington to determine whether the Cave Basalt lavas contain geochemical evidence of substrate contamination by lava erosion. The samples were analyzed using a combination of wavelength-dispersive X-ray fluorescence spectrometry and inductively-coupled plasma mass spectrometry. The results indicate that the oldest, outer lava tube linings in direct contact with the dacitic substrate are contaminated, whereas the younger, inner lava tube linings are uncontaminated and apparently either more evolved or enriched in residual liquid. The most heavily contaminated lavas occur closer to the vent and in steeper parts of the tube system, and the amount of contamination decreases with increasing distance downstream.

These results suggest that erosion by lava and contamination were limited to only the initially emplaced flows and that erosion was localized and enhanced by vigorous laminar flow over steeper slopes. After cooling, the initial Cave Basalt lava flows formed an insulating lining within the tubes that prevented further erosion by later flows. This interpretation is consistent with models of lava erosion that predict higher erosion rates closer to sources and over steeper slopes. A greater abundance of xenoliths and xenocrysts relative to xenomelts in hand samples indicates that mechanical erosion rather than thermal erosion was the dominant erosional process in the Cave Basalt, but further sampling and petrographic analyses must be performed to verify this hypothesis.

Editorial responsibility: J. Donnelly-Nolan

Introduction

Erosion by flowing lava (here termed "lava erosion") has been suggested to occur during the formation of some lava tubes and channels on the terrestrial planets and satellites (e.g., Greeley and Hyde 1972; Hulme 1973, 1982; Carr 1974; Baird 1984; Wilson and Mouginis-Mark 1984, 2001; Baker et al. 1992; Gregg and Greeley 1993; Komatsu et al. 1993; Komatsu and Baker 1994; Bussey et al. 1995; Williams-Jones et al. 1998; McEwen et al. 2000; Williams et al. 2000a, 2000b, 2001a, b, c). Such erosion has two components: thermal erosion and mechanical erosion. Thermal erosion is the partial or wholesale melting of solid or particulate substrate from the heat of the flowing lava, in which part or all of the melted substrate may be incorporated or assimilated into the liquid lava as it travels downstream. Mechanical erosion is the plucking or lifting of partly-consolidated or unconsolidated substrate into the flowing lava. Mechanically eroded material can be melted once it is entrained in the flow if the lava temperature is above the melting temperature of the substrate. The term thermomechanical erosion is often used to describe a combination of both processes. Mathematical modeling has suggested that very low-viscosity lavas, such as Precambrian komatiites, were capable of turbulent flow and substantial thermal erosion of both consolidated and unconsolidated mafic and felsic substrates (Huppert et al. 1984; Huppert and Sparks 1985; Jarvis 1995; Williams et al. 1998, 1999, 2001a), as well as thermomechanical erosion of unconsolidated felsic sediment (Williams et al. 1998, 2001a). Recent modeling has shown that basaltic lavas in the laminar flow regime are capable of substantial thermal erosion of consolidated basalt, assuming long duration flow (i.e., weeks to months: Fagents

and Greeley 2001; Kerr 2001). In contrast, purely mechanical erosion has not been studied rigorously (Ciesla and Keszthelyi 2000).

Field evidence of lava erosion on Earth has been observed and described beneath active tube-fed basalt flows of Kilauea, Hawaii (e.g., Swanson 1973; Coombs et al. 1990; Peterson et al. 1994; Kauahikaua et al. 1998) and active channel-fed carbonatite flows of Oldoinyo Lengai in Tanzania (e.g., Dawson et al. 1990). Also, field evidence has been inferred in prehistoric tube-fed basalt flows in Washington, Oregon, Hawaii, and elsewhere (e.g., Greeley 1971; Greeley and Hyde 1972; Cruikshank and Wood 1972; Wood 1981; Coombs et al. 1990; Greeley et al. 1998) and in Precambrian channel-fed komatiite flows in Australia and Canada (e.g., Huppert et al. 1984; Lesher et al. 1984, 2001a, 2001b; Huppert and Sparks 1985; Groves et al. 1986; Barnes et al. 1988; McNaughton et al. 1988; Evans et al. 1989; Frost and Groves 1989; Houlé et al. 2002). However, much of the field evidence, especially in Precambrian komatiite flows, is equivocal. The search for unequivocal morphological and geochemical evidence of lava erosion is hampered by many factors. Structural deformation and metamorphism of Precambrian komatiites hampers recognition of erosion in most areas. The inaccessibility of lava-substrate contacts beneath active basalt flows makes identification of physical evidence of erosion virtually impossible. Furthermore, active basaltic lava tubes in which thermal erosion has been indirectly observed (e.g., Kauahikaua et al. 1998) tend to be emplaced as parts of growing flow fields. Thermal erosion of older, underlying basalt flows of virtually the same composition does not produce significant geochemical changes. Thus, the best scenario for identifying evidence of lava erosion may be in young (i.e., Holocene), empty tubes where (1) substrate contacts can be studied and sampled, (2) rocks have not been altered, and (3) the substrate is of significantly different chemical composition than the lava. Such localities are very rare.

The Cave Basalt flow, on the southern flank of Mount St. Helens, Washington (Greeley and Hyde 1972; Greeley et al. 1998), provides an excellent opportunity to study erosion of a felsic substrate by a young basaltic lava flow and is, to the best of our knowledge, a unique environment in this respect for tube-fed pahoehoe flows and therefore serves as an important benchmark to investigate these erosional processes. In this paper we review previous studies of physical evidence for lava erosion in the Cave Basalt, discuss our sampling approach, and present the results of our geochemical studies. To the best of our knowledge, this is the first study to attempt to identify geochemical evidence of lava erosion in a Holocene basaltic lava tube system.

Background

The Cave Basalt has been described by Greeley and Hyde (1972), and field evidence for erosion by lava in this area has been summarized by Greeley et al. (1998). The Cave Basalt was originally mapped as an 11-km-long high-Al pahoehoe basalt flow that erupted on the southwestern flank of Mount St. Helens. More recent mapping, however, shows that the Cave Basalt is at least 14 km long, with an origin under younger rocks at an elevation of nearly 5,000 ft. The flow has been dated at ~1900 years B.P. (Greeley and Hyde 1972) and was emplaced in a stream valley incised into dacitic pyroclastic flow and lahar deposits of Mt. St. Helens' Swift Creek and Cougar eruptive stages. A lava tube system covering ~9 km of the Cave Basalt was identified by Halliday (1963), and hosts named tube segments called Little Red River Cave, Ape Cave, Lake Cave, and Ole's Cave (Fig. 1). The longest cave is Ape Cave, which is 3.4 km long. Greeley and Hyde (1972) suggested that lava tube formation included constructional roof accretion over lava channels, influenced by pre-flow topography and thermomechanical erosion of the substrate. Greeley et al.'s (1998) evidence for erosion by lava in this area includes (1) tube segments with undercut cross sections (Fig. 2a) and (2) xenoliths of dacitic country rock incorporated into the tube linings and floors (Fig. 2b, c), which are suggestive of mechanical erosion. Additionally, they noted the presence of glassy dacitic "xenomelts", which appear to consist of melted country rock that resolidified on the tube wall and which can be traced (in a few locations) to their sources behind the lava tube linings (Fig. 2d). These xenomelts are evidence of substrate melting and flow from the heat of the molten basalt in the tubes and demonstrate the potential for thermal erosion to have occurred.

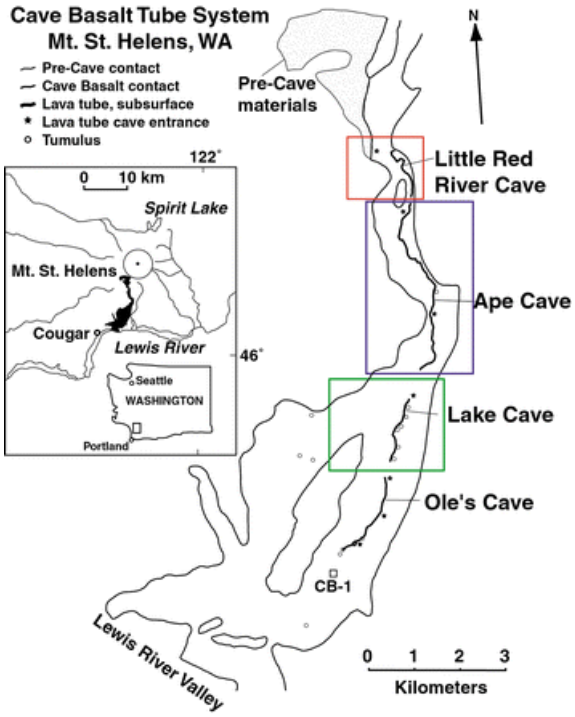

Fig. 1. The Cave Basalt lava tube system, Mount St. Helens, Washington (modified from Greeley and Hyde 1972, and Crandell 1987). *Boxes* refer to expanded views (including sample locations) in Fig. 3. Distribution of the basalt is shown in *black* on the *inset map*

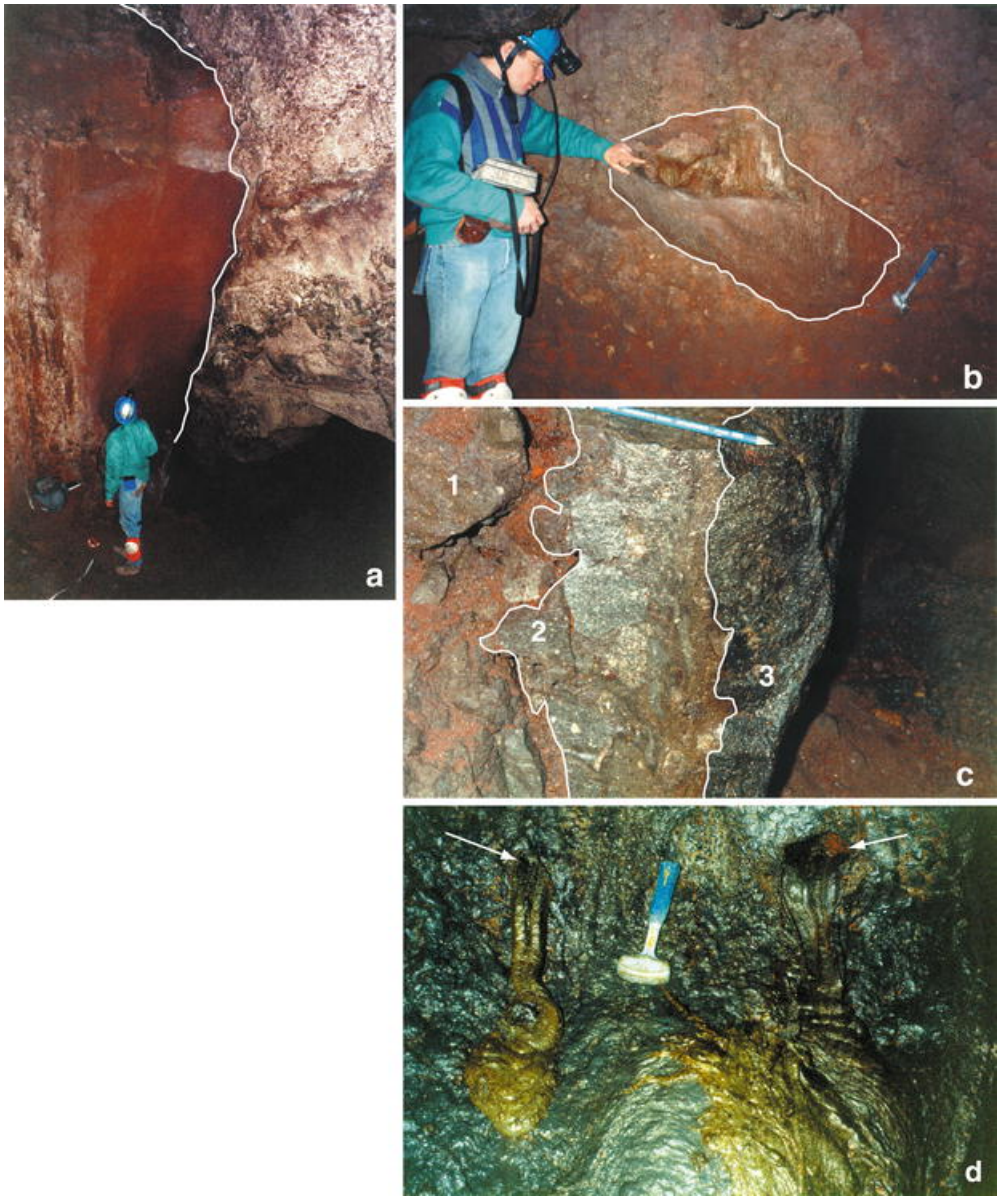

Fig. 2. a Cross section of pre-flow sediments (*left*) in contact (*white line*) with Cave Basalt (*right*) exposed by tube lining breakdown in upper Little Red River Cave. The main tube is the *dark cavity* in *front* and to the *right* of the field assistant. Note the undercutting of the pre-flow material, which is nearly block-free. Vertical erosion at this location is ~15.5 m (Greeley et al. 1998). **b** Meter-sized xenolith of dacite from pyroclastic flows that underlie the Cave Basalt flow, showing partly melted edge in proximity to the tube lining (broken away in this area to expose the block and surrounding pre-flow sediments); the remaining tube lining partly obscures the head of the field assistant, who is pointing to the melted area on the block. The *white line* marks the contact of the xenolith and surrounding sediments. **c** Cross section of the tube lining in Ape Cave showing, from *left* to *right*, (1) baked and partly fused pre-flow sediments, (2) the outer tube lining (*light gray, containing lighter colored xenoliths*), and (3) the inner tube lining (*darker layer on far right*). The combined thickness of the inner and outer tube linings is ~20°cm. *White lines* mark contact boundaries. **d** Green glassy xenomelt produced from pre-flow dacites has drained into the lava tube through

small breaches in the tube lining (*white arrows*). The green color is restricted to the glass coating and is not present in the interior of the samples, which tend to be porphyritic and black in color

---

Petrographically, the Cave Basalt is a porphyritic lava with phenocrysts of olivine and plagioclase in an aphanitic to microcrystalline groundmass. Olivine phenocrysts are typically broken and average 0.5 to 1 mm in length, whereas plagioclase phenocrysts are typically euhedral, zoned (An_{70} to An_{40}), and average 1–2 mm in length (Greeley and Hyde 1972). The phenocryst content of the Cave Basalt is constant throughout the flow field (30–35%), but the groundmass texture varies from aphanitic with abundant microphenocrysts in proximal lavas to microcrystalline in distal lavas. The Cave Basalt at the Lewis River is nearly holocrystalline. Some flow units are vesicular (1–20% of the rock) with spherical vesicles that range from 0.5 to 8 cm in diameter (Greeley and Hyde 1972). The Cave Basalt also has considerable microvesicularity (i.e., vesicles <1 mm diameter) in samples where large vesicles are rare or absent. All flow units have a distinct pahoehoe surface morphology.

Sample collection and analysis

Samples were collected by SDK in May 1994 specifically to address the following key questions regarding lava erosion:

1. Is there any geochemical evidence of contamination of basaltic lavas by felsic substrate?
2. Does the nature or degree of contamination vary with distance from the vent?
3. Is contamination restricted to some portions of the tube system (e.g., floor lavas, tube linings) or is it evenly distributed throughout?

Samples were collected in areas where partial collapse of the tube walls exposed cross-sections of the tube linings and pre-flow deposits exterior to the tube (Table 1; Fig. 3). Samples include (1) interior (inner) and exterior (outer) parts of tube linings, (2) baked sediments in contact with the tube lining, (3) unaltered sediments, and (4) late-stage flows on the tube floor. Samples were also collected from sediments adjacent to the Cave Basalt and from the surface flows of the Cave Basalt to assess if any chemical variations are attributable to equilibrium or fractional crystallization or other processes within flow units.

[Table 1. will appear here. See end of document.]

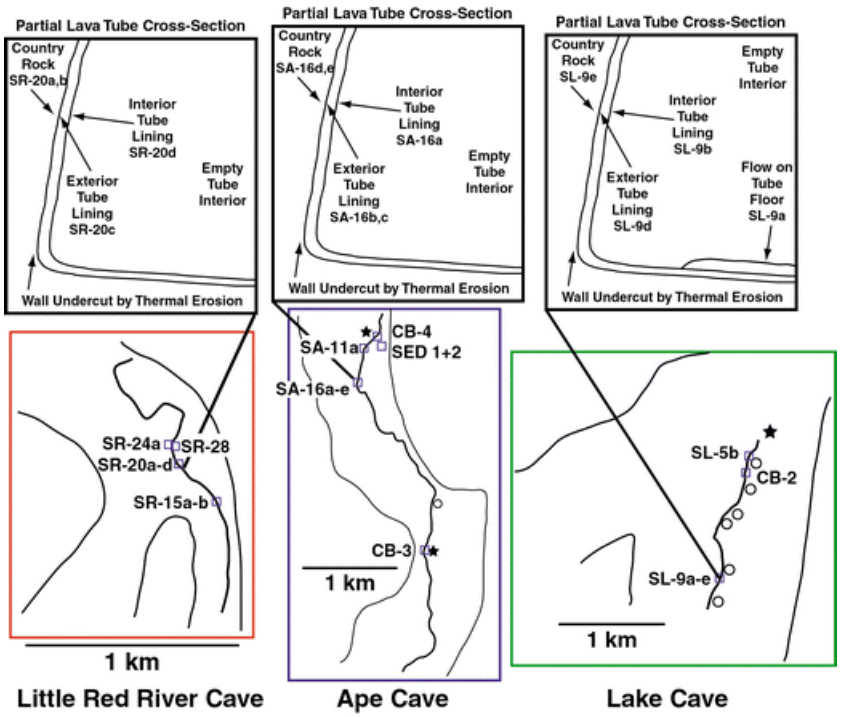

Fig. 3. Locations of collected samples (see also Fig. 1), with schematic cross sections showing the relationships between multiple samples collected at a given location. *Black stars* represent locations of entrances to the lava tube caves, and *circles* represent locations of tumuli mapped by Greeley and Hyde (1972). North is to the *top* on all maps

---

Whole-rock geochemical analyses (Table 2) were performed at the Ontario Geoscience Laboratories in Sudbury, Ontario. Major and minor elements were determined by wavelength-dispersive X-ray fluorescence spectrometry (WD-XRFS) on fused glass disks; routine analytical precision is 3–5% (relative) depending on the abundance of the analyte. Selected trace elements (Cr, V, Rb, Sr, Y, Zr, Nb, Ba, Pb, Zn, Cu, Ni, Co) were determined by WD-XRFS on pressed powder pellets; routine analytical precision is 1–10% (relative), depending on the abundance of the analyte. Additional trace elements (Cs, Rb, Sr, Y, Zr, Nb, Th, U, and rare-earth elements) were determined by inductively-coupled plasma mass spectrometry (ICP-MS) after a 10-day closed-beaker mixed-acid dissolution (Tomlinson et al. 1998); routine analytical precision is 1–10% (relative), depending on the abundance of the analyte.

[Table 2. will appear here. See end of document.]

Results

The geochemical data are given in Table 2 and most samples have been plotted on Harker diagrams (TiO_2, Al_2O_3, Fe_2O_3 total, and MgO vs. SiO_2; Fig. 4), on total alkali (Na_2O+K_2O) vs. silica (SiO_2)

plots (TAS: Le Maitre et al. 1989; Fig. 5), as mantle-normalized incompatible trace element patterns (Fig. 6), and on incompatible trace element ratio plots ($(Th/Nb)_{MN}$ vs. $(La/Sm)_{MN}$: Fig. 7). Because the substrate is compositionally heterogeneous and because contamination may have occurred upstream as well as locally, we have plotted major element data for the local substrate (sample SED 1+2), a substrate sample from the more silica-rich Swift Creek fan, and a substrate sample from the most silica-rich Cougar pyroclastic flows. Previous and unpublished studies have shown that the Cave Basalt has remarkably little compositional variability for a porphyritic arc basalt flow field of its volume, and this statement is supported by our analyses of samples CB-1 through CB-4, which were collected from surface flows near each of the tubes (Fig. 1, 3). We have plotted the inferred composition of the most primitive "uncontaminated" basalt as a series of solid squares using samples CB-1 through CB-4. We have also plotted calculated linear (mechanical) mixing trajectories between uncontaminated basalt (sample CB-4) and "composite" substrate (sample SED1+2) on Figs. 4, 5, and 7. In order to evaluate trends in the data with those produced by equilibrium crystallization (EC) and assimilation-equilibrium crystallization (AEC), we have modeled EC and AEC major element trajectories using MELTS (Ghiorso and Sack 1995) and plotted EC trajectories on Figs. 4, 5 (the AEC trajectories were not significantly different). For these calculations we used sample CB-4 at 1 bar pressure and at a temperature of ~1,160 °C (~30% crystals) as our starting composition. We have also modeled the EC trace element trajectories using the mass balance equation derived by Shaw (1970) and partition coefficients compiled by Rollinson (1993) in Fig. 7.

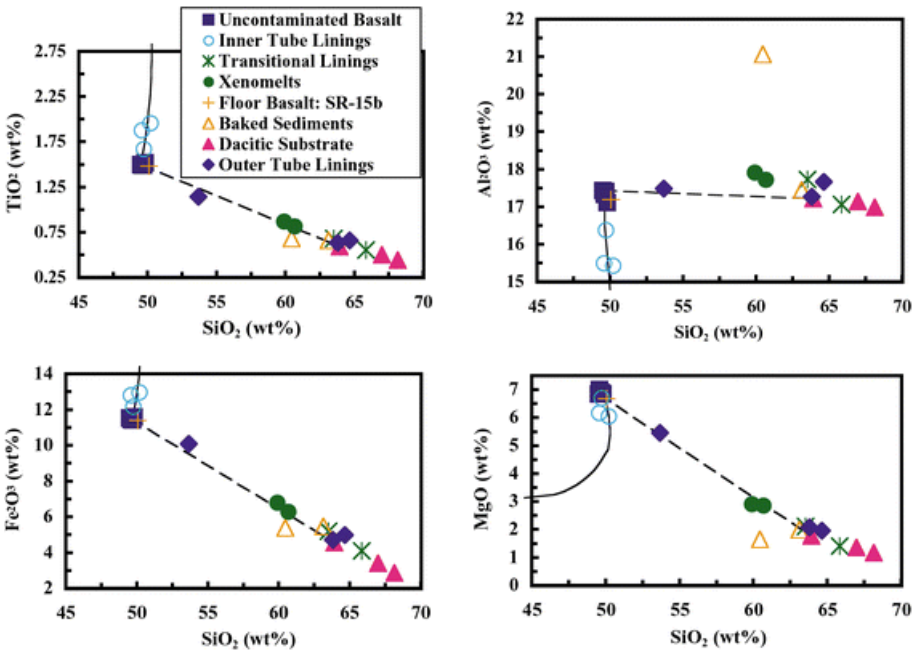

Fig. 4. Selected Harker geochemical plots of major oxides vs. silica (SiO_2) for the Cave Basalt samples. *Clockwise from upper left*: TiO_2, Al_2O_3, Fe_2O_3, and MgO. The *solid line* represents the trend of residual liquid during equilibrium crystallization of lava sample CB-4 as modeled by MELTS (Ghiorso and Sack 1995). The *dashed line* represents the linear mixing trend between "uncontaminated" lava (samples CB-1–4) and "composite" dacitic substrate (sample SED1+2), indicative of lava erosion. The outer lava tube linings that are in direct contact with the country rock appear contaminated, whereas the inner tube linings that had no contact with the country rock are either uncontaminated or are more evolved or enriched in residual liquid. Transitional linings with visible entrained xenoliths and green xenomelts (dacite coatings on basalt) show the expected compositions between lava and substrate

---

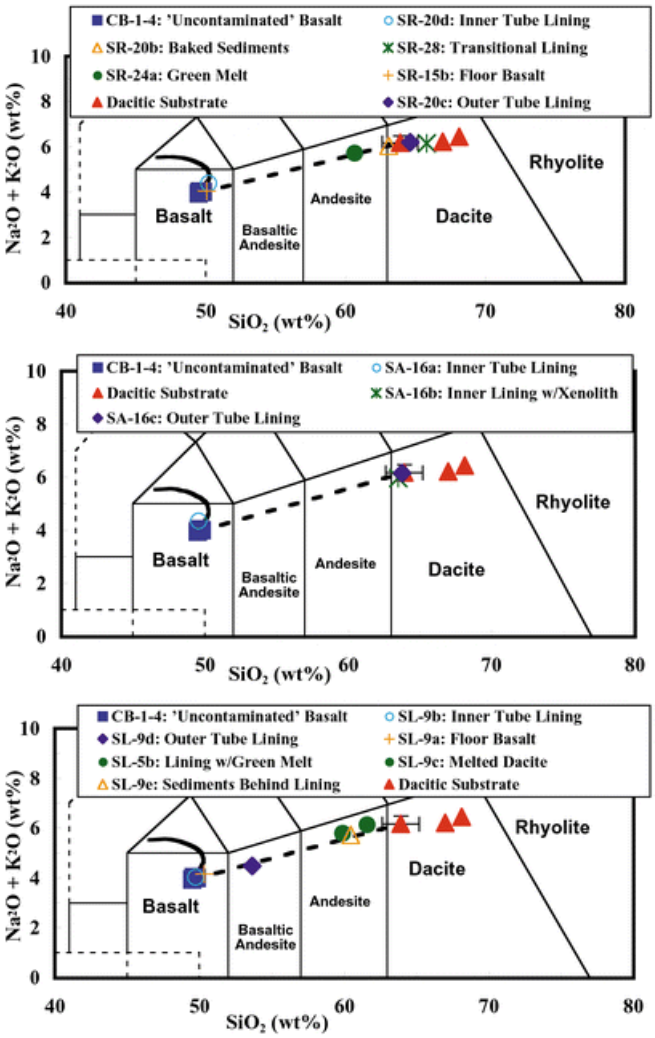

Fig. 5. Total alkalis vs. silica (TAS) plots, modified from Le Maitre et al. (1989), showing uncontaminated Cave Basalt lava (samples CB-1–4), "composite" dacitic substrate (sample SED1+2), and the physical mixing line between them (*dashed line*) indicative of contamination by lava erosion. Representative error bars are 5%, as shown for sample SED1+2. The *solid black line* represents the path of Cave Basalt lava (CB-4) undergoing equilibrium crystallization as modeled by MELTS (Ghiorso and Sack 1995), the trend of which is distinct from that of contamination by lava erosion. Samples are from Little Red River Cave

(*top*), upper Ape Cave (*middle*), and lower Lake Cave (*bottom*). In all plots, the innermost lava tube linings appear to be either uncontaminated lavas, or evolved or enriched in residual liquid, whereas the outer tube linings directly in contact with the substrate appear contaminated. Contamination is greatest closest to the source (Table 1)

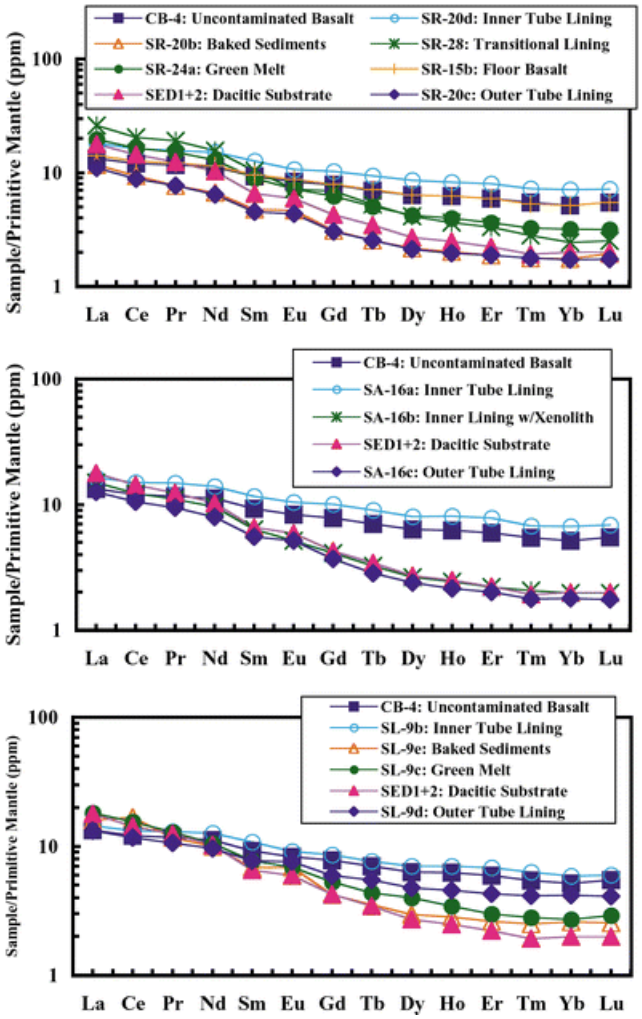

Fig. 6. Mantle-normalized trace element patterns for Cave Basalt samples from Little Red River (*top*), upper Ape (*middle*), and lower Lake Caves (*bottom*). Data normalized using the values for "Primitive Mantle" from McDonough and Sun (1995). The relatively flat patterns of many of the samples are typical of continental basalts. The enrichment in highly incompatible lithophile elements (Th, U, LREE) relative to moderately incompatible lithophile elements (MREE and HREE) and the negative Nb–Ta anomalies in the outer tube linings are consistent with contamination by upper crustal materials, the geochemical signature of erosion by flowing lava

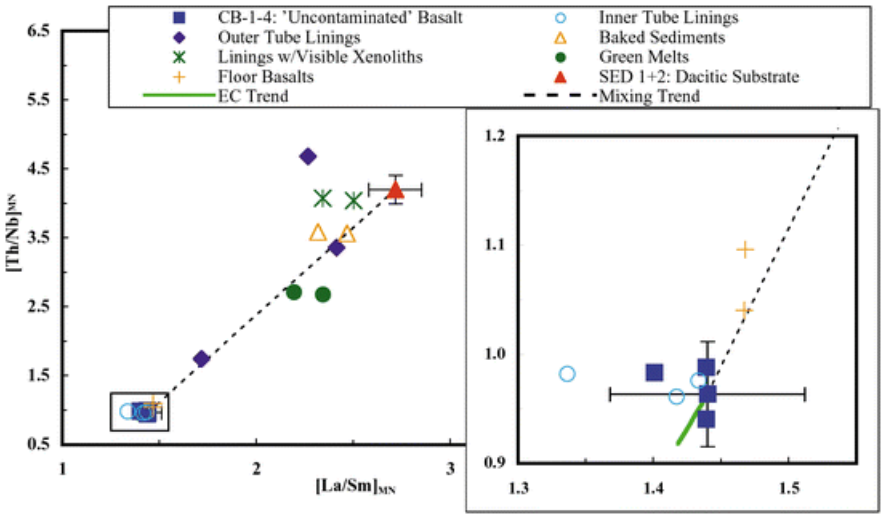

Fig. 7. Incompatible HFS trace element ratio plots—$(Th/Nb)_{mn}$ vs. $(La/Sm)_{mn}$—for Cave Basalt samples. The physical mixing trend due to lava erosion (*dashed line*) is plotted between samples CB-4 (uncontaminated lava) and sample SED1+2 ("composite" substrate). Also included is the calculated trend for equilibrium crystallization (EC) of olivine + plagioclase. Error bars are ±5% on sample CB-4 and SED1+2. The inset plot (*lower right*) is an enlargement of the boxed area around sample CB-4, showing the trends for lava erosion (*dashed line*) and EC (*solid line*). The EC trend was calculated using equation 4.17 and olivine and plagioclase partition coefficients compiled by Rollinson (1993), assuming olivine and plagioclase crystallized in a ratio of ~1:3 (as predicted by MELTS). The trends are consistent with those of the major elements, indicating little or no element mobility by hot fluids that affected the cooling lava and that the compositional variations in the outer tube linings are attributable to physical mixing by mechanical erosion rather than EC. The EC trend is very dependent on the choice of partition coefficient, but calculations using other published partition coefficients indicate that none of the EC trends pass through the contaminated sample compositions

---

The results can be summarized as follows:

1. Inner tube linings (furthest from the country rock) and the late-stage flows on the tube floor are weakly contaminated (<2–6%), or uncontaminated evolved lavas that follow the trend of residual liquid during equilibrium crystallization (Figs. 4, 5). The only sample of an inner tube lining that appears to be contaminated is sample SA-16b from Ape Cave, which contained a visible xenolith of dacite within the analyzed basalt sample, therefore showing that the geochemical signature of contaminated basalt is attributable to the presence of the xenolith. In contrast, the outer tube linings (in direct contact with the country rock) appear to be contaminated by the substrate (~20–80%). Thus, geochemical assimilation by lava erosion apparently took place, but was restricted to the lavas directly in contact with the substrate, which was presumably eroded during initial lava emplacement. As noted by Greeley et al. (1998), some outer linings contain entrained xenoliths and xenocrysts of wall rock, as well as green glassy coatings of

melted dacite (xenomelts), which suggest that both mechanical erosion and thermal erosion operated simultaneously. As expected, lining samples containing visible xenoliths/xenocrysts have a geochemical signature consistent with contamination. Similarly, analyzed samples of basalt tube lining with the green coating (interpreted to be dacitic xenomelt) have a geochemical signature intermediate between basalt and dacite, consistent with the interpretation that the green coating is primarily melted dacite (i.e., green material is ~25% basalt, ~75% dacite). The apparent greater abundance of xenoliths and xenocrysts compared to xenomelts in the Cave Basalt tubes suggests that mechanical erosion was more important than thermal erosion during tube formation, as might be expected in relatively unconsolidated pyroclastic flow substrates.

2. The most heavily contaminated sample of tube lining is from Little Red River Cave, which is closest to the source, and the degree of lava contamination appears to decrease with increasing distance from the vent (Table 1). This trend might seem counterintuitive, as one might expect continuously-flowing, eroding lavas to become increasingly contaminated downstream. However, if the contamination is predominantly local, resulting from incomplete physical mixing between the marginal boundary layer and the inner channel, then greater contamination should be expected closer to the vent. This is consistent with mathematical modeling of lava erosion, in which the highest erosion rates occur closest to the vent (Huppert and Sparks 1985; Williams et al. 1998, 1999, 2001a). Alternatively or additionally, the greater contamination closer to the source could have occurred because of flow over the lava falls and other steeper stretches found in the upper parts of the Cave Basalt tube system (Greeley and Hyde 1972), in which localized flow disruptions could enhance mechanical erosion (e.g., Williams et al. 1999; Fagents and Greeley 2001). This is supported by the presence of visible xenoliths and xenocrysts of substrate in some of the outer linings (Fig. 2b, c) in those areas, indicating mechanical erosion of the substrate. Finally, the most contaminated samples of outer linings could also represent initially-emplaced flows that quickly cooled and insulated the later flows from contact with the substrate, as suggested by Lesher and Arndt (1995) for Archean komatiite lava channels at Kambalda, Western Australia. This hypothesis would also explain the uncontaminated, possibly more evolved flows emplaced on the tube floor, which represent the waning stages of the eruption. These later flows, which only partly fill tubes and were apparently less voluminous than the initial flows, were unable to melt through the existing basaltic linings into the substrate.
3. Major elements are often mobilized when fluids come into contact with hot lavas (e.g., Humphries 1984). However, the rare-earth elements (REE) and high-field strength elements (e.g., Th, Nb), which are much less likely to be mobilized by hot fluids moving through fractures in the cooling

lava, exhibit trends similar to those of the major elements (Figs. 6, 7). That is, the samples from the outer tube linings fall much closer to the trend for physical mixing (lava erosion) than to the trend of residual liquid during equilibrium crystallization (EC). The only exception is sample SA-16c (outer tube lining, Upper Ape Cave: the symbol off the dashed line in Fig. 7), which lies off the mechanical mixing line and is apparently anomalously enriched in La relative to Sm. La is sometimes more mobile than the rest of the LREE (e.g., Layton-Matthews et al. 2003).

Discussion

The compositional evolution of volcanic rocks may be modeled in terms of several end-member processes: fractional crystallization (FC), in which crystallized solids are systematically removed from the evolving liquid, equilibrium crystallization (EC), in which crystallized solids remain in equilibrium with the evolving liquid, and assimilation-fractional crystallization (AFC) or assimilation-equilibrium crystallization (AEC) in which a contaminant is added during FC or EC. Because of the relatively high viscosity of the phenocryst-rich Cave Basalt, FC and AFC are physically unlikely processes, as there is no efficient way for the solid component to be removed, although a physical rearrangement of liquid and crystals could have occurred through filter pressing or flow segregation. As such, we have modeled EC and AEC, instead of FC and AFC, which produce broadly similar geochemical trends except for highly compatible elements (e.g., Ni in olivine) or highly incompatible elements (e.g., alkalis in olivine).

An important aspect of geochemical modeling is the choice of the starting composition. Because the Cave Basalt is porphyritic, it was erupted containing intratelluric phenocrysts rather than as an aphyric lava that crystallized primocrysts. If any crystal sorting has occurred, then the sampled lavas will have different compositions than the erupted lavas. However, if the crystals were not significantly sorted, as argued above, then the bulk composition (groundmass + phenocrysts) should be similar to the erupted composition. One of us (MAC) has suggested that the inner tube linings and the late-stage flows on the tube floors might not be flows that are more evolved by EC, as suggested in Results section, but rather that they are slightly enriched by residual liquid. Such enrichment might occur by migration of a small amount of residual liquid out of the lava during solidification, a process that chemically mimics FC, which is common in less viscous basalts. More detailed petrographic and geochemical studies will be required to better elucidate these processes, but for the purposes of this study, we have assumed that the analyzed composition of sample CB-4 is closest to the erupted composition. Nevertheless, our geochemical modeling

using MELTS shows that the trends in our data are different from those expected from EC, AEC, FC, and AFC, and are mostly likely attributable to mechanical mixing of lava and substrate. Greeley and Hyde (1972) suggested that the Cave Basalts were emplaced as primarily laminar to transitional flows. However, because turbulent flow is much more efficient at removing the lower boundary layer and conducting heat into the substrate (Huppert and Sparks 1985; Williams et al. 1998, 1999, 2001a) and because, with all else equal, this is more likely to occur in areas with steeper slopes (Williams et al. 1999), the geochemical evidence for contamination presented in this paper suggests that locally turbulent flow (which would have entrained unconsolidated dacitic substrate) could have occurred in areas with steeper slopes. It is possible to investigate the emplacement style of the Cave Basalt using its analyzed composition, inferred temperatures using the composition and crystallinity of the lava, estimates of flow thickness based on measurements of lava strand lines and slopes inside the lava tubes, and the analytic equations of Kerr (2001). Table 3 lists the compositions and physical properties of uncontaminated Cave Basalt lava, average substrate, and several other analogs for comparison. Several points worth noting include:

[Table 3. will appear here. See end of document.]

1. Using the major oxide composition of sample CB-4 and average phenocryst content of Cave Basalt lavas (30–35%), we have calculated the liquidus and eruption temperatures using MELTS (Ghiorso and Sack 1995), the lava viscosity using the algorithms of Shaw (1972) and Pinkerton and Stevenson (1992), and lava density using the algorithm of Bottinga and Weill (1970). The calculated bulk viscosities are ~370–570 Pa·s and the bulk density (excluding vesicles) is ~2,510 kg m^{-3}, which are typical values for crystal-rich basalts.
2. Ideally, we would have liked to determine the effect of gas bubbles on viscosity and density, as some of the Cave Basalt flows are vesicular. However, their vesicularity is presently poorly constrained. Qualitatively, the presence of vesicles would be expected to increase viscosity and reduce density, which would reduce the flow velocity, flow rate, and Reynolds number. Thus, the actual values of these parameters would have been somewhat lower than the model values reported in this work.
3. Greeley et al. (1998) reported the average pre-flow slopes in Little Red River, Ape, and Lake Caves to be 4.5°, 3.3°, and 2.6°, respectively. The heights of the lowest lava strand lines above the tube floors (which can be taken as first-order estimates of flow depths in tubes) in Little Red River and Ape Caves range from ~0.8 to 1.6 m. Because downcutting by lava erosion can orphan strand lines above the lava stream and result in inferred lava stream depths that are too

large (Kauahikaua, personal communication, 2002), we have chosen to model flow thickness using conservative values of 0.8 and 1.2 m.

4. At the locations in Little Red River, Upper Ape, and Lower Lake Caves where samples were collected, the corresponding tube widths are 3.8, ~3, and ~5 m, respectively. The emplacement model of Kerr (2001) requires tube widths to be much greater than lava stream depths, however, we do not know of any models for geometries closer to those of the Cave Basalt flows, so the reader should keep these caveats in mind when evaluating our modeling results.

Using the emplacement model of Kerr (2001), the calculated flow velocities, two-dimensional flow rates, and Reynolds numbers (Re) are given in Table 4. These calculations suggest that for a range of flow thicknesses and ground slopes the Cave Basalt lavas were emplaced as laminar flows, as predicted by Greeley and Hyde (1972). Even in locally steeper areas, such as the upper part of Little Red River Cave, where the slope is >10° (Greeley et al., 1998) or the lava fall in Ape Cave, where the slope is ~40°, the crystal-rich, viscous nature of the Cave Basalt probably inhibited turbulent flow.

[Table 4. will appear here. See end of document.]

Implications

The investigation of the processes involved in erosion by flowing lava is complicated because it has been difficult to separate the processes of thermal erosion and mechanical erosion (both in recognition in the field evidence and in development of computer models). In reality, the two processes may be intimately linked, such that both usually occur, but to varying degrees (dependent on local eruption and environmental conditions). In the case of the Cave Basalt, if we assume, as the field evidence and our modeling show, that the lava flows were indeed emplaced as laminar flows, and if our interpretations of the field and geochemical data are correct (i.e., that contamination was caused mostly by physical mixing from mechanical erosion by the initial flows and was strongest closest to the source vent), then this information provides important constraints on the apparent relationship between lava erosion and flow emplacement.

It has been assumed, for example, that terrestrial lava erosion was dominated by thermal erosion rather than mechanical erosion in both the earliest Archean komatiite lavas (Huppert et al. 1984; Huppert and Sparks 1985; Williams et al. 1998) and in recent Hawaiian tube-fed flows (Kauahikaua et al. 1998). This assumption may be attributable in part to the fact that the earliest computer models focused on thermal erosion, which is more straight-forward to model mathematically than

mechanical erosion, and in part to the fact that most inferred erosional channels occur in solid basaltic substrates, where mechanical erosion has been thought to be less effective. In the case of Archean komatiites, the inferred very high eruption temperatures and very low viscosities of komatiite lavas would enable turbulent flow and enhance the potential for thermal erosion in insulated lava tubes and channels (e.g., Huppert et al. 1984; Lesher et al. 1984; Huppert and Sparks 1985; Williams et al. 1998, 1999). In the case of recent Hawaiian flows, the long duration of mostly laminar, tube-fed eruptions (weeks to months) may have enhanced the thermal erosion of underlying basalt flows reported by Kauahikaua et al. (1998). Recent work by Kerr (2001) has shown that substantial thermal erosion should occur in long-lived, laminarly flowing, tube-fed Hawaiian basaltic lavas. Yet the Cave Basalt tubes appear to be dominated by mechanical erosion over thermal erosion. Can we determine the cause of this difference?

We have compared lava flow properties for the Cave Basalt tubes (based on calculations performed for this study) with published values for the tube-fed Hawaiian flows from Kauahikaua et al. (1998) and Kerr (2001) in Table 5. Although there is still considerable uncertainty about some of the Cave Basalt flow properties (particularly the minimum–maximum ranges of flow velocities, flow rates, and eruption durations), the primary differences between the Cave Basalt and the Hawaiian flows is in their bulk viscosities and the nature of their substrates. Because the substrate under the Cave Basalt is unconsolidated to poorly-consolidated tuff (compared to the consolidated basalt flows under the Hawaiian tubes), it was more likely to undergo mechanical erosion rather than thermal erosion. Additionally, the porphyritic, crystal-rich Cave Basalt probably had a higher bulk viscosity than the Hawaiian lavas, which would have resulted in slower flow velocities and lower Reynolds numbers (all else equal). These conditions might also promote mechanical erosion over thermal erosion, although this has yet to be rigorously modeled.

[Table 5. will appear here. See end of document.]

Previous computer modeling by Fagents and Greeley (2001) has shown (for laminar, tube-fed basalt flows over solid basalt substrate at distances of ~8 km downstream from the vent) that sustained flow for a time period of 2 weeks is required to initiate partial melting of the substrate, unless the thermal boundary layer at the base of the flow is disrupted. Such disruption could be caused by topographic irregularities (e.g., lava falls) or by accumulation of rubble on the tube floor during an eruption hiatus (Kauahikaua et al. 1998). If such disruption occurs, unsteady heat transfer in the thermal boundary layer could enhance thermal erosion (Kerr 2001) and if such disruption is caused by rubble on the tube floor, the rubble could be entrained and scour the floor (Kauahikaua et al. 1998), also enhancing erosion, though it would now be thermomechanical erosion. This

appears to be the case in the Kilauea tubes, in which the locations where thermal erosion has been measured (indirectly) are at skylights above lava falls where the flow has been disrupted (Kauahikaua et al. 1998).

This also appears to be the case in the Cave Basalt, in which there is enhanced erosion at breaks in slope where lava falls occur. Once again, the fundamental difference between the two cases appears to be in the physical nature of the substrate: unconsolidated to poorly-consolidated dacitic sediment vs. massive basalt. Dacitic material has a lower melting temperature than basaltic material, so that (without flow disruption) if it takes two weeks to initiate partial melting of basaltic substrate, it should take less time to initiate partial melting of dacitic substrate (all else equal). As the data in Table 5 indicate, there was likely sufficient time to initiate thermal erosion within the Cave Basalt; the fact that substantial thermal erosion apparently did not occur must be due to the rheology of the flow and the physical nature of the substrate.

In the caves studied thus far (Ole's Cave has not yet been sampled), the greater abundance of xenoliths or xenocrysts in tube linings relative to xenomelts and contaminated lavas suggest that mechanical erosion was more important than thermal erosion in producing the contaminated outer tube linings. Interestingly, the amounts of contamination measured in Archean komatiite flows over wet, poorly-consolidated felsic substrates by thermal and thermomechanical erosion (~2–20%: Lesher and Arndt 1995; Barnes et al. 1995) are far less than that measured in the outer Cave Basalt tube linings in this study (~20–80%), which presumably resulted from mostly mechanical erosion. However, these estimates from mixing lines are rather crude, and better data will be obtained from future petrographic analyses. From such analyses the relative abundances of xenoliths, xenocrysts, and xenomelts can be assessed at the microscopic scale, which we plan to do as part of a more comprehensive sampling of the Cave Basalt flow field (including Ole's Cave and the distal flows) as future work. Nevertheless, this study has shown that the Cave Basalt has a unique potential to provide insight into the processes of lava erosion and the dynamics of tube-fed lava flow emplacement.

Summary and conclusions

Geochemical analyses of basaltic lavas and underlying dacitic country rocks indicate that the oldest, outer lava tube linings of the Cave Basalts on Mt. St. Helens are contaminated by dacitic substrates, whereas the youngest, inner lava tube linings are uncontaminated, but likely either enriched by residual liquid or more evolved lavas by equilibrium crystallization. The most

strongly-contaminated lavas occur closer to the vent and in steeper parts of the tube system, suggesting that greater degrees of erosion occurred proximal to the vent in steeper areas. Available data suggest that the Cave Basalt flows were laminar in nature, consistent with mathematical models of erosion by flowing lava. Mechanical erosion rather than thermal erosion appears to have been the dominant erosional process in the Cave Basalt, but further sampling and analyses must be performed to verify this conclusion.

Acknowledgments We are grateful to Jim Nieland (Gifford Pinchot National Forest Service office) for granting S.D.K. permission to collect samples in the Cave Basalt lava tubes and to Greg Michaels (ASU) for assistance with the fieldwork in 1994. We are also grateful to Paul Neumann (MERC) for preparing the samples for geochemical analyses, Ray Gorzynksi (MERC) for performing the dissolutions for ICP-MS analysis, and Marcus Burnham (OGL) for supervising the ICP-MS analyses. The authors would like to thank Jim Kauahikaua and Steve Self for very helpful reviews of the manuscript, which significantly improved the final version. Julie Donnelly-Nolan provided detailed editorial comments that have enhanced this paper. This work was funded by grants from the Planetary Geology and Geophysics Program (NASA) to RG and from the Natural Sciences and Engineering Research Council of Canada (NSERC) to CML.

References

Arndt NT (1976) Melting relations of ultramafic lavas (komatiites) at one atmosphere and high pressure. Carnegie Institute Geophysical Laboratory Yearbook 75, Carnegie Institute, Washington, DC, pp 555–562

Baird AK (1984) Did komatiitic lavas erode channels on Mars? Nature 311:18

Baker VR, Komatsu G, Parker TJ, Gulick VC, Kargel JS, Lewis JS (1992) Channels and valleys on Venus: preliminary analysis of Magellan data. J Geophys Res 97:13421–13444

Barnes SJ, Coats CJA, Naldrett AJ (1982) Petrogenesis of a Proterozoic nickel sulfide-komatiite association: the Katiniq Sill, Ungava, Quebec. Econ Geol 77:413–429

Barnes SJ, Hill RET, Gole MJ (1988) The Perseverance Ultramafic Complex, Western Australia: The product of a komatiite lava river. J Petrol 29:302–331

Barnes SJ, Lesher CM, Keays RR (1995) Geochemistry of mineralized and barren komatiites from the Perseverance nickel deposit, Western Australia. Lithos 34:209–234

Bottinga Y, Weill DF (1970) Densities of liquid silicate systems calculated from partial molar volumes of oxide components. Am J Sci 269:169–182

Bussey DBJ, Sørensen S-A, Guest JE (1995) Factors influencing the capability of lava to erode its substrate: application to Venus. J Geophys Res 100:16941–16948

Carr MH (1974) The role of lava erosion in the formation of lunar rilles and Martian channels. Icarus 22:1–23

Ciesla FJ, Keszthelyi L (2000) A simple model for lava flow quarrying: mechanical erosion of substrate. In: Lunar Planet Sci XXXI, Abstract No1,647, Lunar and Planetary Institute, Houston, Texas (CD-ROM)

Coombs CR, Hawke BR, Wilson L (1990) Terrestrial analogs to lunar sinuous rilles: Kauhako crater and channel, Kalaupapa, Molokai, and other Hawaiian lava conduit systems. In: Proceedings of the 20th Lunar Planetary Science Conference, Lunar Planetary Institute, Houston, Texas, pp 195–206

Cruikshank DP, Wood CA (1972) Lunar rilles and Hawaiian volcanic features: possible analogs. Moon 3:412–447

Crandell DR (1987) Deposits of pre-1980 pyroclastic flows and lahars from Mount St. Helens volcano, Washington. US Geol Surv Prof Pap 1444, US Geol Surv, Reston, Virginia, 91 pp

Dawson JB, Pinkerton H, Norton GE, Pyle DM (1990) Physicochemical properties of alkali carbonatite lavas: data from the 1988 eruption of Oldoinyo Lengai, Tanzania. Geology 18:260–263

Evans DM, Cowden A, Barratt RM (1989) Deformation and thermal erosion at the Foster nickel deposit, Kambalda-St. Ives, Western Australia. In: Prendergast MD, Jones MJ (eds) Magmatic sulphides: the Zimbabwe volume, Inst of Miner and Metall, London, pp 215–219

Fagents SA, Greeley R (2001) Factors influencing lava-substrate heat transfer and implications for thermomechanical erosion. Bull Volcanol 62:519–532

Frost KM, Groves DI (1989) Ocellar units at Kambalda: evidence for sediment assimilation by komatiite lavas. Prendergast MD, Jones MJ (eds) Magmatic sulphides: the Zimbabwe volume. Inst of Miner and Metall, London, pp 207–213

Ghiorso MS, Sack RO (1995) Chemical mass transfer in magmatic processes IV. A revised and internally consistent thermodynamic model for the interpolation and extrapolation of liquid–solid equilibria in magmatic systems at elevated temperatures and pressures. Contrib Mineral Petrol 119:197–212

Greeley R (1971) Observations of actively forming lava tubes and associated structures, Hawaii. Mod Geol 2:207–223

Greeley R, Hyde JH (1972) Lava tubes of the Cave Basalt, Mount St. Helens, Washington. Geol Soc Am Bull 83:2397–2418

Greeley R, Fagents SA, Harris RS, Kadel SD, Williams DA, and Guest JE (1998) Erosion by flowing lava: field evidence. J Geophys Res 103:27325–27345

Gregg TKP, Greeley R (1993), Formation of Venusian canali: considerations of lava types and their thermal behaviors. J Geophys Res 98:10873–10882

Groves DI, Korkiakoski EA, McNaughton NJ, Lesher CM, and Cowden A (1986) Thermal erosion by komatiites at Kambalda, Western Australia and the genesis of nickel ores. Nature 319:136–139

Halliday WR (1963) Caves of Washington. Wash Div of Mines and Geol, Olympia, Inf Circ 40, pp 71–104

Houlé MG, Lesher CM, Davis PC, Sproule RA, Montgomery JK (2002) Thermomechanical erosion of footwall andesites by komatiites at the Alexo Ni–Cu–(PGE) deposit, Abitibi Greenstone Belt, Canada. In: Proceedings of the 9th International Platinum Symposium, Billings, Montana, pp 189–192

Hulme G (1973) Turbulent lava flows and the formation of lunar sinuous rilles. Mod Geol 4:107–117

Hulme G (1982) A review of lava flow processes related to the formation of lunar sinuous rilles. Geophys Surv 5:245–279

Humphries SE (1984) The mobility of the rare earth elements in the crust. Henderson P (ed) Rare earth element geochemistry. Elsevier, Amsterdam, pp 315–341

Huppert HE, Sparks RSJ (1985) Komatiites I: eruption and flow. J Petrol 26:694–725

Huppert HE, Sparks RSJ, Turner JS and Arndt NT (1984) Emplacement and cooling of komatiite lavas. Nature 309:19–22

Jarvis RA (1995) On the cross-sectional geometry of thermal erosion channels formed by turbulent lava flows. J Geophys Res 100:10127–10140

Kauahikaua JP, Mangan M, Heliker CC, and Mattox T (1996) A quantitative look at the demise of a basaltic vent: The death of Kupaianaha, Kilauea Volcano, Hawaii. Bull Volcanol 57:641–648

Kauahikaua J, Cashman KV, Mattox TN, Hon KA, Heliker CC, Mangan MT, and Thornber CR (1998) Observations on basaltic lava streams in tubes from Kilauea volcano, Hawaii. J Geophys Res 103:27303–27324

Kerr RC (2001) Thermal erosion by laminar lava flows. J Geophys Res 106:26453–26465

Komatsu G, Baker VR (1994) Meander properties of Venusian channels. Geology 22:67–70

Komatsu G, Baker VR, Gulick VC, Parker TJ (1993) Venusian channels and valleys: distribution and volcanological implications. Icarus 102:1–25

Lange RA, Navrotsky A (1992) Heat capacities of Fe2O3-bearing silicate liquids. Contrib Mineral Petrol 110:311–320

Layton-Matthews DM, Burnham OM, Lesher CM (2003) Trace element geochemistry of ultramafic intrusions in the Thompson Nickel Belt: relative roles of contamination and metasomatism, Gangue 76:(1)4–10

Le Maitre RW, 10 coauthors (1989) A classification of igneous rocks and glossary of terms, Blackwell, Oxford

Lesher CM, Arndt NT (1995) Trace element and Nd isotope geochemistry, petrogenesis, and volcanic evolution of contaminated komatiites at Kambalda, Western Australia. Lithos 34:127–157

Lesher CM, Arndt NT, Groves DI (1984) Genesis of komatiite-associated nickel sulphide deposits at Kambalda, Western Australia: a distal volcanic model. In: Buchanan DL, Jones MJ (eds) Sulphide deposits in mafic and ultramafic rocks. Inst Miner Metal, London, pp 70–80

Lesher CM, Burnham OM (2001a) Multicomponent elemental and isotopic mixing in Ni–Cu–(PGE) ores at Kambalda, Western Australia. Can Mineral 39:421–446

Lesher CM, Burnham OM, Keays RR, Barnes SJ, Hulbert L (2001b) Trace-element geochemistry and petrogenesis of barren and ore-associated komatiites. Can Mineral 39:673–696

McEwen AS, 25 coauthors (2000) Galileo at Io: results from high-resolution imaging. Science 288:1193–1198

McDonough WF, Sun, S-S (1995) The composition of the Earth. Chem Geol 120:223–253

McNaughton NJ, Frost KM, Groves DI (1988) Ground melting and ocellar komatiites: a lead isotopic study at Kambalda, Western Australia. Geol Mag 125:285–295

Murase T, McBirney AR (1973) Properties of some common igneous rocks and their melts at high temperatures. Geol Soc Am Bull 84:3563–3592

Navrotsky A (1995) Energetics of silicate melts. In: Stebbins JF, McMillan PF, Dingwell DB (eds) Structure, dynamics and properties of silicate melts. Rev Mineral 32:121–142

Nichols GT, Wyllie PJ, Stern CR (1996) Experimental melting of pelagic sediment, constraints relevant to subduction. In: Bebout, GE, Scholl DW, Kirby SH, Platt JP (eds) Subduction top to bottom. Am Geophys Un Geophys Mon 96, Washington, DC, pp 293–298

Peterson DW, Holcomb RT, Tilling RI, Christiansen RL (1994) Development of lava tubes in the light of observations at Mauna Ulu, Kilauea Volcano, Hawaii. Bull Volcanol 56:343–360

Pinkerton H, Stevenson RJ (1992) Methods of determining the rheological properties of magmas at subliquidus temperatures. J Volcanol Geotherm Res 53:47–66

Rollinson HR (1993) Using geochemical data: evaluation, presentation, interpretation. Longman, Essex, pp 102–170

Shaw DM (1970) Trace element fractionation during anatexis. Geochim Cosmochim Acta 34:237–243.

Shaw HR (1972) Viscosities of magmatic silicate liquids: an empirical method of prediction. Am J Sci 272:870–893

Swanson DA (1973) Pahoehoe flows from the 1969–1971 Mauna Ulu eruption, Kilauea Volcano, Hawaii. Geol Soc Am Bull 84:615–626

Tomlinson KY, Bowins R, Hechler J (1998) Refinement of hafnium (Hf) and zirconium (Zr) ICP-MS analyses by improvement in the sample digestion procedure. In: Summary of fieldwork and other activities. Miscellaneous Pap No 169, Ontario Geological Survey, Toronto, pp 189–192

Williams DA, Kerr RC, Lesher CM (1998) Emplacement and erosion by Archean komatiite lava flows at Kambalda: revisited. J Geophys Res 103:27533–27550

Williams DA, Kerr RC, Lesher CM (1999) Thermal and fluid dynamics of komatiitic lavas associated with magmatic Ni–Cu–(PGE) sulphide deposits. In: Keays RR, Lesher CM, Lightfoot PC, Farrow CEG (eds) Dynamic processes in magmatic ore deposits and their application in mineral exploration. Short Course, No 13, Geological Association of Canada, St. John's, Newfoundland, pp 367–412

Williams DA, Wilson AH, Greeley R (2000a) A komatiite analog to potential ultramafic materials on Io. J Geophys Res 105:1671–1684

Williams DA, Fagents SA, Greeley R (2000b) A reevaluation of the emplacement and erosional potential of turbulent, low-viscosity lavas on the Moon. J Geophys Res 105:20189–20206

Williams DA, Kerr RC, Lesher CM, Barnes SJ (2001a) Analytical/numerical modeling of komatiite lava emplacement and thermal erosion at Perseverance, Western Australia. J Volcanol Geotherm Res 110/1–2:27–55

Williams DA, Davies AG, Keszthelyi LP, Greeley R (2001b) The July 1997 eruption at Pillan Patera on Io: implications for ultrabasic lava flow emplacement. J Geophys Res 106:33105–33119

Williams DA, Greeley R, Lopes RMC, Davies AG (2001c) Evaluation of sulfur flow emplacement on Io from Galileo data and numerical modeling. J Geophys Res 106:33161–33174

Williams-Jones G, Williams-Jones AE, Stix J (1998) The nature and origin of Venusian canali. J Geophys Res 103:8545–8555

Wilson L, Mouginis-Mark P (1984) Martian sinuous rilles. Lunar Planet Sci XV, 926–927

Wilson L, Mouginis-Mark PJ (2001) Estimation of volcanic eruptions conditions for a large flank event on Elysium Mons, Mars. J Geophys Res 106:20621–20628

Wood C (1981) Exploration and geology of some lava tube caves on the Hawaiian volcanoes. Trans Br Cave Res Assoc 8:111–129

Table 1. Lava samples collected in and around the Cave Basalt lava tube system, Mount. St. Helens, Washington

Sample no.	Sample description	Approx. sample location elevation (ft)[a]	Relative contamination (%)[b]
Little Red River Cave			
SR-24a	Green xenomelt from base of lava fall in Little Red River Cave	2,710	77
SR-28	Outer tube lining, further down-tube, with distinct xenoliths (i.e., contains apparent physical mixing of basalt with phenocrysts from the dacitic pre-flow substrate)	2,710	112
SR-20a	Sediments and cobbles behind outer tube lining	2,680	N/a
SR-20b	Baked/fused pre-flow sediments and cobbles in contact with outer tube lining	2,680	94
SR-20c	Outer tube lining	2,680	104
SR-20d	Inner tube lining	2,680	6
SR-15a	Glazed/glassy basalt sample of inner tube lining	2,640	4
SR-15b	Basalt sample from flow on tube floor	2,640	4
Ape Cave			
CB-4	Basalt sample from surface flow at upper entrance	2,460	0
SED 1+2	Composite of two samples of dacitic ash and block flow sediments in hillside just east of upper entrance (pre-flow substrate material)	2,460	100
SA-11a	Layered or “bedded” country rock underlying outer tube lining; one of the two pieces was in contact with tube floor material (vesicular sample)	2,430	N/a
SA-16a	Inner tube lining	2,360	2
SA-16b	Inner portion of outer tube lining containing xenolith	2,360	97
SA-16c	Outer portion of outer tube lining in contact with baked pre-flow sediments	2,360	98
SA-16d	Partially fused baked soil	2,360	N/a
SA-16e	Relatively unconsolidated pre-flow sediments (dacite block and ash)	2,360	N/a

Sample no.	Sample description	Approx. sample location elevation (ft)[a]	Relative contamination (%)[b]
CB-3	Basalt sample from surface flow at lower entrance	2,090	0
Lake Cave			
SL-5b	Crystal-rich outer tube lining containing green melted material, upper Lake Cave	1,830	84
CB-2	Basalt sample from surface flow	1,820	0
SL-9a	Basalt sample from flow on floor, lower Lake Cave	1,680	6
SL-9b	Inner tube lining, lower Lake Cave	1,680	2
SL-9c	Green xenomelt, lower Lake Cave	1,680	73
SL-9d	Outer tube lining, lower Lake Cave	1,680	28
SL-9e	Baked sediments underlying outer tube lining, lower Lake Cave (~20 m upflow)	1,680	N/a
Other samples			
CB-1	Basalt sample from block in tumulus near the distal flow margin	1,200	0

Note: All samples are located on Fig. 3 except sample CB-1, which is located on Fig. 1

[a]The exact vent location is unknown, but is thought to be near the 5,000-ft elevation

[b]Calculated using the mixing lines in Fig. 5, in which 0% is represented by samples CB-1–4 (uncontaminated basalt) and 100% is represented by sample SED1+2 (pure substrate). Some samples showing >100% contamination indicate that the local substrate is more felsic than sample SED1+2 on the mixing lines, demonstrating the heterogeneity of the substrate. If calculated using the most silicic sample SC01-426 as 100%, then outer tube linings show contamination between 24–82%. N/a=Not applicable

Table 2. Geochemical data for samples collected from the Cave Basalt lava tube system, Mount St. Helens, Washington. Analyses performed at the Ontario Geoscience Laboratories in Sudbury, Ontario, using WD-XRFS and ICP-MS. Data reported to routine analytical precision of 2σ for amounts present. Samples in order of decreasing elevation and increasing distance from the Cave Basalt source vent (refer to Figs. 1 and 3)

	SR-24a	SR-28	SR-20a	SR-20b	SR-20c	SR-20d	SR-15a	SR-15b	CB-4	SED 1+2	SA-11a	SA-16a	SA-16b	SA-16c	SA-16d	SA-16e	CB-3	SL-5b	CB-2	SL-9a	SL-9b	SL-9c	SL-9d	SL-9e	CB-1
SiO_2 (wt%)	60.7	65.8	63.4	63.1	64.7	50.2	49.8	50.1	49.5	63.9	49.7	49.6	63.5	63.8	62.5	63.4	49.6	61.6	49.8	50.3	49.7	59.9	53.7	60.5	49.7
TiO_2	0.82	0.55	0.66	0.66	0.66	1.96	1.67	1.48	1.50	0.59	0.89	1.88	0.68	0.63	0.67	0.66	1.49	0.87	1.52	1.47	1.67	0.87	1.14	0.68	1.49
Al_2O_3	17.7	17.1	17.6	17.4	17.7	15.4	16.4	17.2	17.4	17.2	17.1	15.5	17.7	17.3	17.6	17.6	17.3	16.7	17.1	17.2	16.4	17.9	17.5	21.1	17.4
Fe_2O_3	6.29	4.10	4.99	5.46	4.99	13.0	12.2	11.4	11.5	4.55	10.6	12.8	5.19	4.72	5.01	4.97	11.4	6.14	11.6	11.8	12.2	6.81	10.1	5.37	11.4
MnO	0.10	0.07	0.08	0.08	0.08	0.19	0.18	0.17	0.16	0.08	0.16	0.19	0.08	0.07	0.08	0.08	0.17	0.10	0.17	0.17	0.18	0.10	0.14	0.07	0.17
MgO	2.87	1.40	1.93	1.99	1.96	6.06	6.51	6.68	6.85	1.77	9.38	6.17	2.11	2.08	2.09	2.03	7.00	2.21	6.85	6.32	6.71	2.91	5.45	1.65	6.90
CaO	5.76	4.05	4.70	4.60	4.69	9.17	9.54	9.37	9.64	4.33	9.75	9.42	4.78	5.10	4.87	4.98	9.74	4.95	9.48	9.13	9.47	5.81	7.94	4.25	9.68
Na_2O	4.59	4.60	4.68	4.65	4.76	3.73	3.64	3.51	3.44	4.71	3.23	3.72	4.61	4.75	4.62	4.69	3.53	4.73	3.46	3.60	3.50	4.65	3.77	4.59	3.49
K_2O	1.13	1.55	1.39	1.40	1.43	0.68	0.56	0.54	0.50	1.46	0.29	0.63	1.36	1.41	1.34	1.36	0.50	1.42	0.54	0.56	0.54	1.15	0.71	1.14	0.51
P_2O_5	0.14	0.12	0.12	0.12	0.14	0.22	0.18	0.17	0.17	0.13	0.10	0.21	0.13	0.13	0.11	0.11	0.16	0.18	0.17	0.17	0.18	0.16	0.15	0.15	0.17
LOI	0.13	<0.01	0.38	0.40	0.17	<0.01	<0.01	<0.01	<0.01	0.78	<0.01	0.23	0.28	0.31	0.23	0.21	<0.01	0.31	<0.01	0.06	<0.01	0.12	<0.01	0.33	<0.01
Total	100.2	99.4	99.9	99.9	101.2	100.7	100.5	100.6	100.6	99.5	100.9	100.3	100.5	100.3	99.1	100.1	100.5	99.2	100.5	100.8	100.5	100.4	100.3	99.8	100.5
Rb (ppm)	27.0	37.5	31.3	31.1	33.6	13.6	11.4	10.8	9.7	31.1	4.8	12.6	27.6	26.3	26.0	26.1	9.27	33.1	10.0	11.6	10.8	26.6	15.4	26.6	9.44
Cs	1.65	1.44	0.98	1.17	1.01	0.52	0.42	0.43	0.36	0.97	0.18	0.45	1.52	0.97	0.94	0.98	0.33	1.50	0.39	0.49	0.42	1.07	0.71	1.39	0.36
Sr	518	529	544	533	558	313	344	356	354	560	349	322	627	657	644	663	342	488	343	361	341	490	393	564	346
La	12.7	16.9	6.6	7.6	7.1	11.7	9.9	9.1	8.6	11.5	4.7	10.6	9.65	8.14	8.06	9.53	8.27	11.7	8.89	8.95	9.32	11.7	8.59	10.3	8.63
Ce	27.4	34.1	14.1	15.8	14.8	27.2	23.2	21.1	20.2	24.0	11.1	25.0	20.6	17.5	17.1	20.2	19.5	23.3	21.1	20.8	22.1	25.9	19.5	28.0	20.7
Pr	3.83	4.82	1.77	1.95	1.95	3.95	3.43	3.09	2.96	3.15	1.67	3.77	2.80	2.39	2.31	2.65	2.85	2.96	3.10	3.06	3.28	3.27	2.68	2.97	2.99
Nd	16.2	19.5	7.4	8.3	8.0	18.9	15.9	14.3	14.0	12.8	7.9	17.4	12.0	9.92	9.54	10.8	13.5	12.0	14.4	14.0	15.8	13.1	12.0	12.4	14.1
Sm	3.62	4.22	1.74	1.93	1.84	5.11	4.30	3.89	3.75	2.66	2.18	4.70	2.58	2.25	2.09	2.41	3.60	2.63	3.87	3.82	4.37	3.13	3.13	2.78	3.86
Eu	1.10	1.10	0.66	0.72	0.67	1.64	1.42	1.35	1.28	0.91	0.89	1.60	0.79	0.79	0.72	0.86	1.31	0.98	1.38	1.34	1.40	1.06	1.17	1.06	1.35
Gd	3.39	3.74	1.50	1.69	1.65	5.59	4.85	4.30	4.25	2.31	2.50	5.48	2.23	2.01	1.91	2.09	4.11	2.45	4.44	4.13	4.67	2.87	3.23	2.28	4.37
Tb	0.50	0.52	0.23	0.25	0.25	0.93	0.77	0.70	0.69	0.34	0.43	0.89	0.33	0.28	0.29	0.30	0.69	0.37	0.72	0.68	0.77	0.43	0.54	0.35	0.70

	SR-24a	SR-28	SR-20a	SR-20b	SR-20c	SR-20d	SR-15a	SR-15b	CB-4	SED 1+2	SA-11a	SA-16a	SA-16b	SA-16c	SA-16d	SA-16e	CB-3	SL-5b	CB-2	SL-9a	SL-9b	SL-9c	SL-9d	SL-9e	CB-1
Dy	2.83	2.78	1.31	1.46	1.42	5.76	4.83	4.27	4.26	1.82	2.55	5.42	1.78	1.60	1.58	1.65	4.28	2.18	4.54	4.09	4.73	2.68	3.20	1.99	4.44
Ho	0.59	0.54	0.27	0.30	0.29	1.23	1.051	0.93	0.93	0.37	0.55	1.20	0.36	0.33	0.33	0.33	0.91	0.45	0.97	0.90	1.04	0.51	0.68	0.42	0.95
Er	1.59	1.45	0.77	0.82	0.82	3.51	2.88	2.59	2.61	0.97	1.59	3.40	0.96	0.88	0.88	0.93	2.60	1.21	2.73	2.55	2.99	1.31	1.88	1.14	2.69
Tm	0.22	0.19	0.11	0.12	0.12	0.49	0.41	0.36	0.37	0.13	0.22	0.46	0.14	0.12	0.12	0.13	0.38	0.18	0.39	0.35	0.43	0.19	0.29	0.17	0.40
Yb	1.40	1.07	0.72	0.77	0.76	3.12	2.56	2.27	2.27	0.88	1.38	2.96	0.87	0.79	0.73	0.78	2.33	1.18	2.40	2.30	2.60	1.19	1.84	1.14	2.38
Lu	0.21	0.17	0.11	0.13	0.12	0.48	0.40	0.37	0.37	0.13	0.21	0.46	0.13	0.12	0.12	0.12	0.36	0.19	0.36	0.35	0.40	0.20	0.28	0.17	0.37
Y	16.6	17.2	7.5	8.1	8.1	33.8	28.6	25.1	25.0	10.2	14.7	31.8	10.1	8.76	8.62	9.09	24.7	12.8	25.1	24.3	29.2	13.7	18.8	10.2	25.6
Zr	102	89.0	105	109	106	150	121	109	110	81.5	59.8	139	108	102	104	105	109	124	110	112	120	101	105	111	110
Hf	3.05	2.88	3.19	3.21	3.15	4.12	3.31	3.01	3.12	2.64	1.77	3.85	3.35	3.10	3.20	3.28	3.03	3.64	3.20	3.07	3.31	3.07	2.81	3.38	3.08
Nb	6.52	5.86	6.04	5.69	5.95	10.6	8.36	7.72	7.82	4.91	3.84	9.73	4.78	3.91	4.71	4.60	7.57	8.68	7.71	7.78	8.26	6.08	6.56	7.038	7.58
Ta	0.39	0.31	0.44	0.35	0.35	0.61	0.49	0.42	0.38	0.27	0.16	0.49	0.26	0.22	0.25	0.25	0.38	0.49	0.40	0.39	0.42	0.35	0.35	0.45	0.39
Th	2.14	2.86	2.19	2.45	2.41	1.25	1.04	0.97	0.91	2.49	0.47	1.13	2.35	2.21	2.29	2.45	0.86	2.42	0.92	1.031	0.99	1.97	1.38	3.050	0.90
U	0.90	1.29	1.10	1.08	1.10	0.48	0.40	0.37	0.35	1.06	0.19	0.44	1.09	0.96	0.94	0.97	0.34	1.028	0.37	0.44	0.39	0.86	0.58	1.21	0.37

Table 3. Modeled thermal/rheological properties for the Cave Basalt, substrate, and other basalts

Component/parameter	Cave Basalt lava	Dacitic tuff substrate	Tholeiitic continental flood basalt	Katinniq komatiitic basalt
SiO_2	49.5	63.9	50.9	46.9
TiO_2	1.50	0.59	1.7	0.6
Al_2O_3	17.4	17.2	14.6	9.8
Fe_2O_3	11.5	0.74	–	–
FeO	0.0	3.43	14.6	14.4
MnO	0.16	0.08	–	0.3
MgO	6.85	1.77	4.8	18.9
CaO	9.64	4.33	8.7	8.6
Na_2O	3.44	4.71	3.1	0.3
K_2O	0.50	1.46	0.8	0.05
P_2O_5	<0.01	0.78	-	0.2
H_2O	<0.01	<0.01	<0.01	<0.01
T_{liq} (°C)	1,205	1,144	1,160	1,419
T_{sol} or T_{mg} (°C)	1,050	950	1,080	1,150
Crystallinity (X, %)	30–35	N.G.	N.G.	N.G.
T_{erup} (°C)	1,160–1,153	N.G.	N.G.	N.G.
ρ_b @ T_{erup} (kg/m^3)	2,510	N.G.	N.G.	N.G.
c (J/kg·°C)	1,560	1,480	1,470	1,640
μ_1 @ T_{erup} (Pa·s)	63–68	21,550 @ T_{liq}	86 @ T_{liq}	0.81 @ T_{liq}
μ_b @ T_{erup} (Pa·s)	370–570	N.G.	N.G.	N.G.
L @ T_{liq} (J/kg)	5.01E+05	2.03E+05	5.37E+05	5.96E+05
Reference[a]	Sample CB-4	Sample SED1+2	1	2

Liquidus temperatures (T_{liq}) were calculated using MELTS (Ghiorso and Sack 1995); the solidus temperatures (T_{sol}) for komatiitic basalt and tholeiitic basalt are taken from the experimental data of Arndt (1976); and the melting temperature (T_{mg}) of felsic sediment is from Nichols et al. (1996). Crystallinity (X) was estimated from the percentage of phenocrysts in several thin sections, and eruption temperature was estimated by the relation $T_{erup}=T_{sol}+X(T_{liq}-T_{sol})$. Bulk density ($\rho_b$) was calculated using the method of Bottinga and Weill (1970) for the liquid, plus 30% plagioclase and olivine crystals; liquid viscosity (μ) was calculated using the method of Shaw (1972) and bulk viscosity was calculated using equations from Pinkerton and Stevenson (1992); specific heat (c) was calculated from the heat capacity data of Lange and Navrotsky (1992); and heat of fusion (L) is approximated using data from Navrotsky (1995). N.G., Not given

[a]1, Columbia River basalt (Murase and McBirney 1973); 2, Katinniq komatiitic basalt (Barnes et al. 1982)

Table 4. Model flow velocities, flow rates and Reynolds numbers for the Cave Basalt lava flows, Mount St. Helens

	Slope=2.6°	Slope=3.3°	Slope=4.5°	Slope=10°	Slope=40°
Flow thickness=0.8 m, crystallinity=30%					
Flow velocity (m/s)	0.96	1.2	1.7	3.7	14
Flow rate (m^2/s)	0.51	0.65	0.88	2.0	7.2
Reynolds number	3.4	4.4	6.0	13	49
Flow thickness=1.2 m, crystallinity=30%					
Flow velocity (m/s)	2.2	2.7	3.7	8.3	31
Flow rate (m^2/s)	1.7	2.2	3.0	6.6	24
Reynolds number	12	15	20	44	170
Flow thickness=0.8 m, crystallinity=35%					
Flow velocity (m/s)	0.63	0.79	1.1	2.4	8.9
Flow rate (m^2/s)	0.33	0.42	0.58	1.3	4.7
Reynolds number	1.5	1.9	2.5	5.6	21
Flow thickness=1.2 m, crystallinity=35%					
Flow velocity (m/s)	1.4	1.8	2.4	5.4	20
Flow rate (m^2/s)	1.1	1.4	1.9	4.3	16
Reynolds number	5.0	6.3	8.6	19	70

Calculations based on lava parameters for composition CB-4 given in Table 3. Flow velocity, flow rate, and Reynolds numbers (Re) calculated using Eqs. (2), (3), and (4) of Kerr (2001). Laminar flow occurs for Re <500, transitional flow occurs for 2000> Re >500, and turbulent flow occurs for Re >2000.

Table 5. Comparison of properties between Cave Basalt lava tubes and Kilauea lava tubes

Parameter	Cave Basalt, Mount St. Helens, Washington	Kupaianaha, Kilauea, Hawaii
Volcano type	Stratovolcano	Shield volcano
Lava composition	Basalt	Basalt
Substrate composition	Dacitic tuff	Basalt
Substrate consolidation	Unconsolidated to poorly-consolidated	Consolidated
Flow field length (km)	~14	11.3
Ground slope (°)	2.6–4.5 (3.5)	2–4.5 (3; Kerr 2001)
Tube interior widths (m)	3–5 (4)	3–10 (4; Kerr 2001)
Inferred flow thicknesses (m)	0.8–1.6 (1)	1–2 (0.7; Kerr 2001)
Lava temperature (°C)	1,160–1,153 (1157)	1,154 (Kerr 2001)
Inferred lava bulk viscosity (Pa s)	370−570 (450)	80 (Kerr 2001)
Estimated flow velocities (m/s)	0.63−6.6 (1.7)	2.5 (Kerr 2001)
Reynolds number	1.5−48 (6.4)	23 (Kerr 2001)
Flow regime	Laminar	Laminar
Estimated flow rates (m^3/s)	1.5–53 (6.6)	3.5 (Kauahikaua et al. 1996)
Estimated eruption durations (months)	1.8–62 (14)	67 (Episode 48)
Estimated total flow volumes (km^3)	0.24	0.60 (Calculated from above data)

Parameters for the Cave Basalt based on modeling from data reported in this study; a range of values are reported for some parameters that represent minimums–maximums, with a “typical” intermediate value given in parentheses. For the Kupaianaha flows, all data are from Kauahikaua et al. (1998) unless otherwise indicated